Available online at www.sciencedirect.com
SCIENCE DIRECT®
ELSEVIER
Earth and Planetary Science Letters 210 (2003) 411–424
EPSL
www.elsevier.com/locate/epsl

Dynamics of the gas flux from shallow gas hydrate deposits: interaction between oily hydrate bubbles and the oceanic environment

Ira Leifer [a,*], Ian MacDonald [b]

[a] *Marine Sciences Institute and Chemical Engineering Department, University of California, Santa Barbara, CA 93106-5080, USA*
[b] *Physical and Life Sciences, Texas A&M University, Corpus Christi, TX 78412, USA*

Received 23 August 2002; received in revised form 19 February 2003; accepted 27 March 2003

Abstract

Decomposition of methane hydrates on the continental margins is a potentially significant source of atmospheric methane, but the input depends upon the poorly understood fate of the hydrocarbon bubbles rising from the sea floor. During a field trip to the Gulf of Mexico, three different seepages were imaged and analyzed. Three different imaging techniques were tried (side, front, and back illumination), of which back illumination produced the best results. The images were analyzed and the size-dependent bubble distribution, mass flux, and rise speeds determined. The total observed gas flux was 62.3×10^{-3} mol s^{-1}, primarily methane, of which a single vent produced seven times the next largest vent. Of this major vent, 50% of the bubble mass was contained in the largest bubbles, $r>5500$ μm. The vertical velocities demonstrated that these bubbles were heavily contaminated with oil, which was also corroborated by bubble shape and oscillation observations.
© 2003 Elsevier Science B.V. All rights reserved.

Keywords: bubble; hydrocarbon seepage; oil; upwelling; bubble size spectra; methane

1. Introduction

In this paper, we report preliminary assessment of bubbly emissions from gas hydrate deposits found at hydrocarbon seeps on the Gulf of Mexico continental slope. The results include quantification from direct observation of rising gas bubbles or oil. The findings pertain to research on the methane flux from decomposing gas hydrate. The magnitude of natural methane emissions has been widely cited as a driving factor for climate change [1,2]. The prevalence of gas hydrate deposits on continental margins [3,4] and the likelihood that these deposits would decompose in response to elevated water temperature or lowered sea-level [5] indicate that this pool of hydrocarbons could provide a large source for rapid methane emission. Global scale decomposition of oceanic gas hydrate has been cited as a possible cause of the latest Paleocene thermal maximum [6]. Recent findings suggest that methane emitted from gas hydrate has influenced Quaternary climate cycles [7]. Processes that constrain gas flux from gas hy-

* Corresponding author. Tel.: +1-805-893-4931; Fax: +1-805-893-4731.
E-mail address: ira.leifer@bubbleology.com (I. Leifer).

0012-821X/03/$ – see front matter © 2003 Elsevier Science B.V. All rights reserved.
doi:10.1016/S0012-821X(03)00173-0

drate deposits in the marine setting are of interest because they affect the fate of hydrate-bound hydrocarbons.

We propose that rapid gas flux from gas hydrate involves the following steps: (1) formation of bubbles at an orifice in the deposit or the sediment overlaying the deposit, (2) interaction of bubbles with possible contaminants, (3) buoyant transit of bubbles through the water column, and (4) gas exchange with the water column through the bubble interface. Transient re-formation of gas hydrate may also occur at the bubble–water interface during rise through the water column [8]. Because the rise speed and gas exchange efficiency of bubbles vary dramatically with size, the fate of methane bubbles depends strongly upon their sizes. Furthermore, this fate also depends upon the release depth and other environmental factors, most of which are poorly constrained. Smaller bubbles are likely to dissolve, while larger bubbles may reach the surface, releasing a fraction of their initial methane to the atmosphere [9]. However, measured size spectra of seep bubbles have been previously unavailable in the published literature.

Bubble behavior is strongly affected by contamination by surfactants – surface active substances. So the interaction of surfactants and seep bubbles is an important consideration in this work. Surfactants influence the hydrodynamic properties of bubbles and hence their rise speed and gas exchange efficiency [10]. Crude oil is a prevalent component of emissions from Gulf of Mexico hydrocarbon seeps [11,12] and represents an obvious source of surfactant contamination in hydrate gas releases. Oil releases from seeps create distinctive features (slicks) on the ocean surface that are often visible in remote sensing images [13,14]. Natural oil slicks provide a dramatic demonstration that some fraction of seeping hydrocarbons escapes the water column and reach the atmosphere. In sufficient quantities, oil also reduces the buoyancy of contaminated bubbles. However, although combined gas and oil flows from Gulf of Mexico seeps have been described [15–17] the phenomenon has not been studied in detail. Better understanding of how oil and gas interact could lead to improved monitoring of natural seeps or accidental oil spills with remote sensing data.

2. Setting and experimental description

2.1. Methane hydrate at the sites

Field work was conducted at two well-known hydrocarbon seeps located in 525–550 m water depths south of Louisiana (Fig. 1). These sites, referred to hereafter as GC185 (27°46.9′N, 91°30.4′W) and GC234 (27°44.1′N, 91°13.1′W), support lush colonies of chemosynthetic tube worms, methanotrophic mussels, and associated invertebrates [18,19]. The fauna provides a distinctive visual cue for locating active seepage. Gas hydrates at these sites occur predominantly in a structure II lattice style [20] that includes thermogenic methane and propane, as well as traces of other hydrocarbon gases [21]. Structure II hydrate remains stable at higher temperatures and lower pressures than pure methane in a structure I lattice style [20]. The gas hydrate layers may be buried under several meters of sediment in these localities [11], but the deposits we investigated were semi-circular mounds in which gas hydrate was immediately evident either as an impenetrable layer beneath a few centimeters of sediment or directly exposed to seawater on the mound edges [21]. Bubble plumes were clearly visible issuing from the hydrate mounds and through a mixture of carbonate rubble and shells in adjacent areas. Gas hydrate mounds at GC185 trap volumes of crude oil in underlying sediments [15]. The oil can be released when the gas hydrate layers are disturbed. Oil droplets seen during the field study were darker, rose more slowly, and were less visible than gas bubbles.

The hydrate mounds were sampled with use of the submarine *Johnson Sea Link I*, a 4-person, battery-operated craft deployed from the research vessel *Edwin Link*. The *Sea Link* recorded color video images from a Sony DXC-3000A three-chip CCD video camera fitted with a Canon J8x6KRS 6–48 mm focal length lens. The nominal frame rate was 29.7 s^{-1}. Images of rising bubble plumes were obtained from GC185 and GC234. A variety of lighting and camera arrangements were used to visualize the rising bubbles (see below). Gas samples were collected in bell jars while gas hydrate samples were recovered in a specially designed

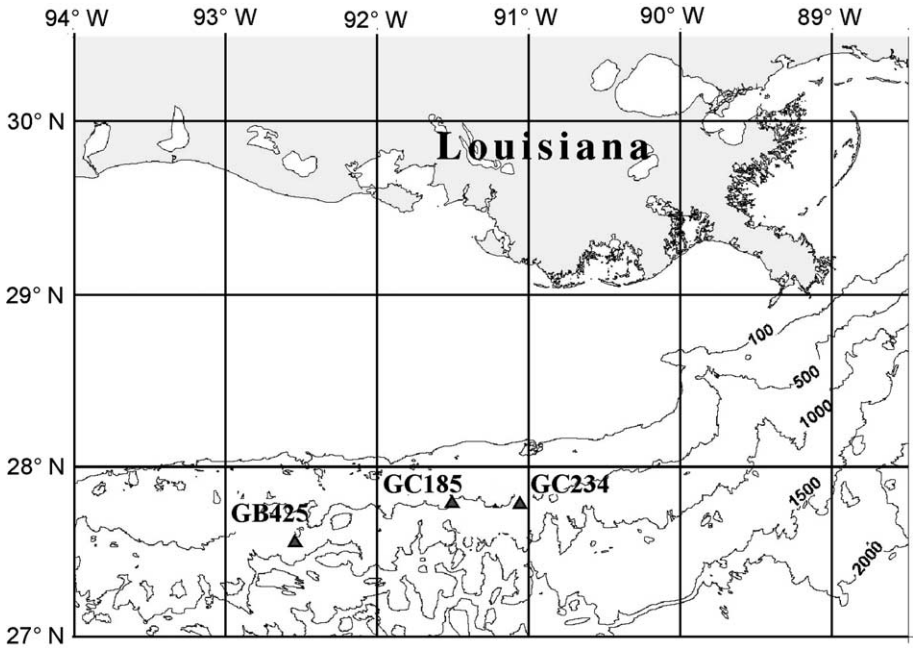

Fig. 1. Study area map showing location of sites GC185 and GC234 in northern Gulf of Mexico southeast of Mississippi River Delta.

container that could be sealed to preserve the material at in situ temperature and pressure [21].

Gas hydrate recovered from GC185 and GC234 was yellowish orange colored (Plate 1h). The discoloration was due to quantities of crude oil that perfuse the gas hydrate mass and remained as a residue when samples of gas hydrate were allowed to completely dissociate. Oil samples were analyzed by gas chromatography with flame ionized detection. Chromatographs showed an oil fingerprint (Fig. 2) consistent with a crude oil partially degraded by bacterial oxidation [22]. Drops of oil were released in situ whenever gas hydrate surfaces were disturbed, e.g., by drilling.

The presence of oil 'contamination' on bubbles observed at the seeps was inferred from the appearance of the bubbles and their oscillatory behavior as they rose through the water, and then confirmed by their rise velocity. Reference images of oily and non-oily bubbles were taken to facilitate comparison (Plate 1a and b). Bubbles were created by forcing air through a drawn glass capillary tube in a tank of fresh water. An oil–gas–water mixture was wicked through the tube to produce oily bubbles. Clean bubbles tended to oscillate rapidly while rising and to flatten into arch-like shapes in their vertical cross-section. Oily bubbles rose without rapid oscillations and were significantly more ellipsoidal in cross-section than non-oily bubbles.

2.2. Bubble visualization and analysis

The intent of bubble visualization was to record a video sequence showing the bubbles next to a calibrated scale of known size and to provide sufficient illumination to distinctly render each bubble (i.e., no motion blur) in the individual video frames. Bubble visualization requires the depth of field to be sufficient to maintain good focus for bubbles in the plume. However, bubble sizing errors can become significant if the bubble plume occupies too large a cross-section of the camera's field of view because the accuracy of size estimation depends upon distance between the size reference and the measured bubble. For broad plumes, baffles can be used to block off all the bubbles outside of a narrow plane. Baffles were not neces-

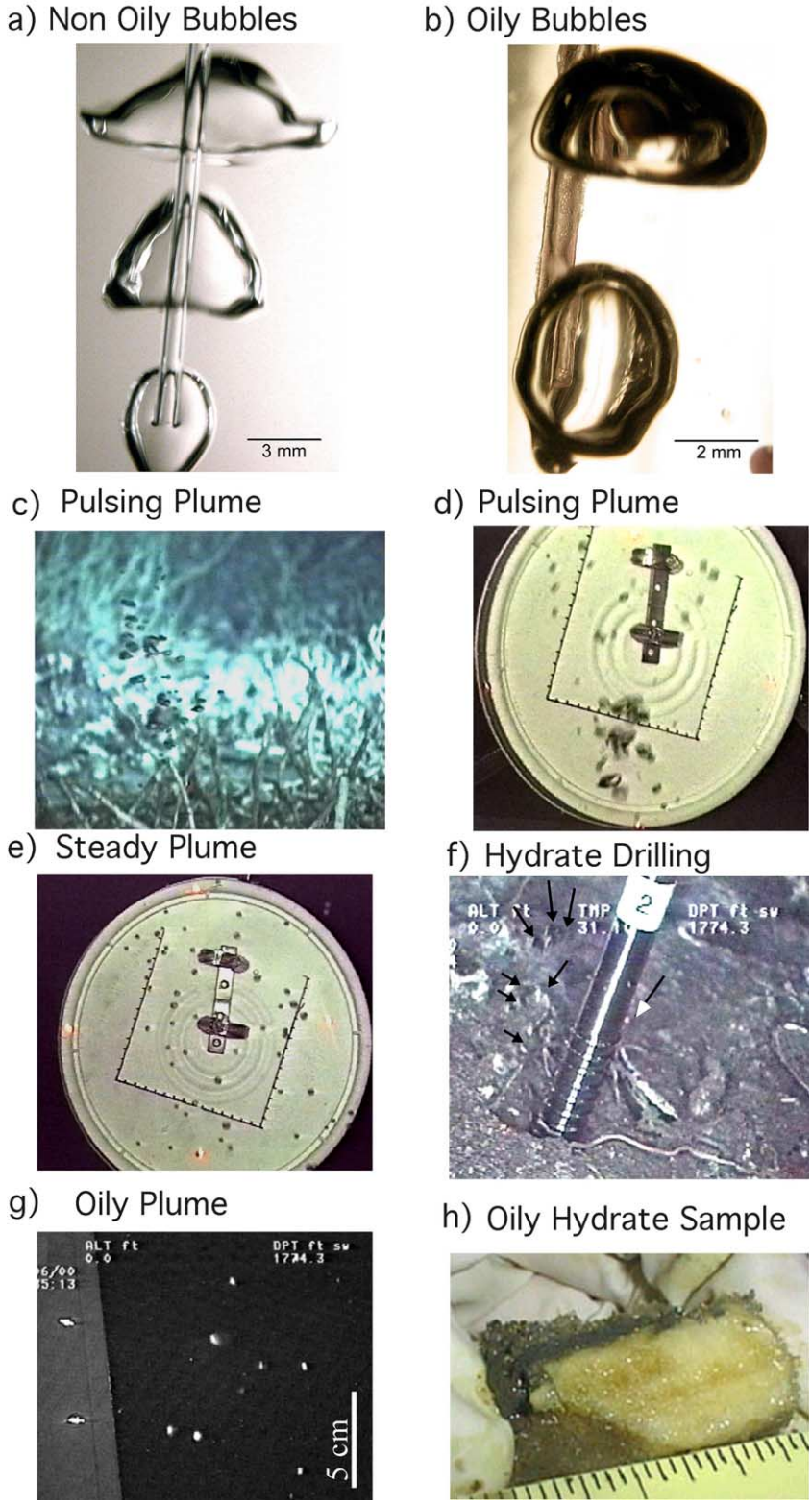
a) Non Oily Bubbles
3 mm
b) Oily Bubbles
2 mm
c) Pulsing Plume
d) Pulsing Plume
e) Steady Plume
f) Hydrate Drilling
ALT ft
0.0
TMP
31.1
2
DPT ft sw
1774.3
g) Oily Plume
ALT ft
0.0
DPT ft sw
1774.3
5 cm
h) Oily Hydrate Sample

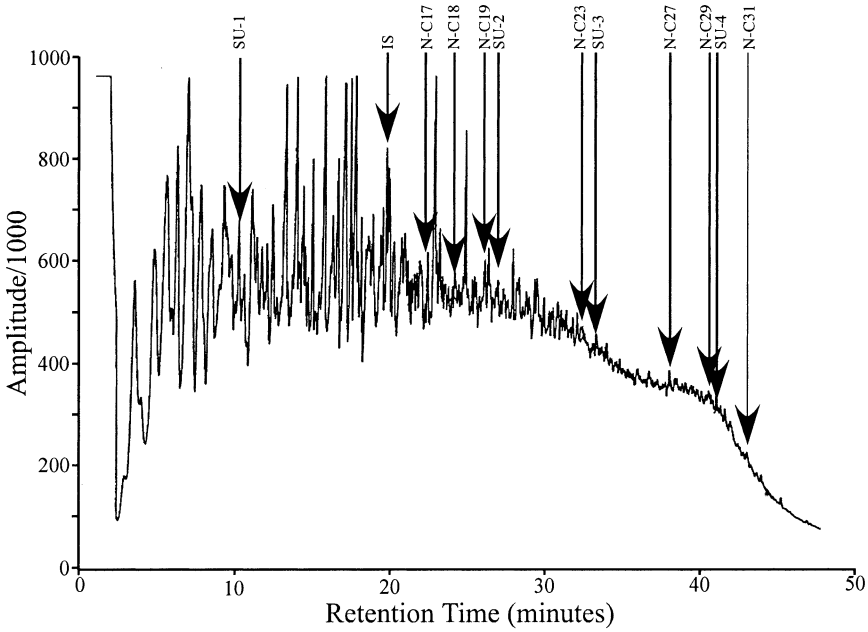

Fig. 2. Gas chromatograph with flame ionized detection showing whole oil residue from gas hydrate sample.

sary for the bubble plumes we measured. Imaging a bubble with distinct edges requires a shutter speed sufficiently fast to freeze bubble motion. For auto-iris video cameras, this requires sufficient illumination to force the shutter speed. Three illumination schemes were attempted in the present observations. With front illumination, the principal light sources were quartz flood lamps mounted in the same plane as the camera. For side illumination, a collimated light source was placed perpendicular to the camera's point of view and immediately adjacent to the bubble plume. For back illumination, lamps placed behind the camera plane were reflected back into the bubbles by a white panel placed immediately behind the bubble plume.

A summary of each bubble plume's characteristics and the illumination techniques used is presented in Table 1a and b. In the three illumination techniques, the auto-iris shutter speed of the video camera was too slow (due to insufficient illumination) and bubbles appeared as streaks (Plate 1d). This problem was partially overcome when the submersible was able to rise with the bubbles so that the relative velocity between the bubbles and camera was small. Back illumination provided the best results, with in-focus bubbles showing as dark outlines with bright centers. With back illumination, the white panel had markings to indicate size scale (Plate Ie). Side illumination with the collimated light source provided images that were the most difficult to analyze. Bubbles appeared as half moons with the dark side edge extremely difficult to distinguish, and required hand

←

Plate I. (a) Clean bubble of air in fresh water. (b) Bubble of air with addition of oil. (c) Back-lit image of pulsing bubble plume with white plastic panel for scale (tick marks are 1 cm). (d) Back-lit image of steady bubble plume. (e) Bubbles (black arrows) and small hydrate pieces released by drilling into surface deposit of gas hydrate. Bubble plume is front-lit. Drill bit is 2.5 cm in diameter. (f) Side-lit plume of oily bubbles released from drilling operation. (g) Small sample of gas hydrate recovered from sea floor deposits in study area. Crude oil inclusions are clearly visible as linear streaking and yellowish discoloration throughout sample.

analysis. Although for spherical bubbles it was easy to estimate the far edge, for the irregular shapes of most of the larger seep bubbles, this was difficult, thereby increasing the sizing uncertainty. Bolts on the collimated light source were used for size scale (Plate 1g). Front illumination provided two difficulties, it was almost impossible to determine if a bubble was in focus, and secondly, bubble edges were less distinct. Size comparison for bubbles that initially were front illuminated, and then back illuminated (by rising above the panel top) showed that front illumination underestimated bubble size. Front illumination also worked best with a black background.

Using routines written in NIH Image [23] bubbles were outlined and the best-fit ellipse (least-squares, linear-regression analysis of the angle, major, and minor axes) was determined for each bubble. Streaked bubbles, touching bubbles, and obscured bubbles were outlined by hand. Where possible, bubbles were outlined by defining the edge after applying a binary threshold [24]. The threshold level was chosen close to the local background intensity [25]. Tracking bubbles from one frame to the next helped identify obscured bubbles. All bubbles visualized with the collimated light source were hand outlined. The size-dependent vertical velocity was calculated for each bubble stream by the expedient method of counting the number of frames a bubble required to rise 20 cm.

From the best-fit ellipse, the equivalent spherical radius, r, was calculated by [26]:

$$r = (r_a^2 r_b)^{1/3} \quad (1)$$

where r_a is the radius along the major axis and r_b is the radius along the minor axis. Then the bubble number size distribution, N (number in the field of view during the sequence per size unit increment), was calculated from a histogram of the time series of r, using logarithmically spaced bin widths. This was then converted into the layer size population, Φ (μm^{-1} m^{-1}) and the emission flux size distribution Ψ (μm^{-1} s^{-1}). Each serves a different purpose, for example, the layer distribution is an instantaneous snapshot and thus is what a sonar observes, while the emission flux can be used to initialize a bubble model, or calculate the molar flux to the sea surface. Although bubble size distributions normally are reported as a concentration (μm^{-1} cm^{-3}); due to plume inhomogeneity (i.e., it is local) the plume horizontal dimensions (width and breadth) are required to make the concentration useful. Instead, we avoid this added complexity by reporting the bubble population, or the total number of bubbles in a layer or flux for the entire plume.

Calculation of Φ is:

$$\Phi = \{N/\Delta r\}/\{F_N(H-4r)/\cos(\theta)\} \quad (2)$$

where Δr is the logarithmically varying bin width, r is the equivalent spherical radius, F_N is the number of frames in the image sequence, H is the height of the field of view, and θ is the camera tilt angle from vertical. The equation above assumes that bubbles touching the edge are not counted. To calculate Φ for a 1-cm thick layer, both H and r must be in centimeters. The emission flux, Ψ, is the number of bubbles of each size that cross an arbitrary horizontal plane, say the image bottom per second in each r bin, and is:

$$\Psi = \{N/\Delta r\} \times \{V_Z(r)/[R \times ((H-4r)/\cos(\theta))]\} \times [R/F_N] \quad (3)$$

where $V_Z(r)$ is the velocity profile and R is the frame rate (the units are frames per second). The term $\{V_Z(r)/[R \times ((H-4r)/\cos(\theta))]\}$ is a correction term and represents the (mean) time for a bubble of a certain size to rise across the field of

Table 1a
Summary of observations and illumination and analysis techniques for bubble plumes observed at Bush Hill

Stream name	Flow type	Illumination technique	Analysis technique	Oiliness	Spectrum
Pulsing	pulsing	back-lit	hand/thresh	minimal	broad
Steady	continuous	back-lit	hand/thresh	oily	narrow
Oily	continuous	collimated light	hand	extreme	narrow

view, and thus the number of times a bubble is counted. From Φ and Ψ, the mass distribution, Φ_M (mol μm^{-1} m^{-1}) and mass emission flux distribution, Ψ_M (mol μm^{-1} s^{-1}), can be calculated using the equivalent spherical volume, V, defined by $V = (4/3)\pi r^3$ and the ideal gas law, $n = PV/RT$, where P is the hydrostatic pressure, n is the molar content, R is the universal gas constant, and T is the temperature.

Bubble distributions from breaking waves are generally described by a power law dependency [27,28]:

$$\Phi(r,t) \sim r^{-S_L}, \quad \Psi(r,t) \sim r^{-S_F} \tag{4}$$

where t is time, and S_L and S_F are the power law exponents for the layer and flux distributions, respectively. Values of S were calculated by linear-regression analysis of the log of both sides of Eq. 4 over an appropriate size range, indicated in each figure. Errors were calculated as $N^{-0.5}$ where N is the number of bubbles in each r bin. Actual errors were somewhat larger since each bubble was measured multiple times.

3. Results

3.1. Stream emission description

At GC185, two bubble plumes were visible rising from locations a few meters apart. One of the plumes seemed to consist of a relatively constant flux of bubbles while the other produced distinct pulses of bubbles. The steady plume emanated from a small fissure in the sediment covering the hydrate mound. On close inspection, the bubbles were seen issuing from the exposed surface of the hydrate. The pulsing plume rose largely unobstructed from an overhanging mouth that collected bubbles causing the pulsating release. The pulsing bubble plume is shown in Plate 1d, which also shows the plastic panel used to provide back illumination. In contrast, the steady bubble plume (Plate 1e) was observed rising from a bed of tube worms and mussels. Either the absence of an overhang, or break-up by the fauna caused the bubbles to be continuously emitted.

Video sequences of each of these bubble plumes were digitized and analyzed. Representative images are shown in Plate 1. Bubble streaking due to slow shutter speed was severe for the pulsing plume (Plate 1d), and analysis was entirely by hand. Bubble streaking was significantly less for the steady plume (Plate 1e) where illumination was greater, and rise velocities were less than for the pulsing plume. When digital thresholding was able to discriminate the bubbles from the background, analysis was automated using image processing routines. However, non-discriminated, touching, and obscured bubbles were outlined manually. As can be seen, the smallest bubbles were quite large, $r \sim 1000$–2000 μm, with many significantly larger, up to 2 cm in diameter. Larger bubbles generally tend to flatten due to hydrodynamic forces as they rise [10]. Thus it is interesting that many of the largest bubbles were ellipsoidal or nearly spherical. One explanation, supported by further evidence presented below, is that larger bubbles were highly contaminated by oil.

3.2. Vertical velocities of the bubbles

The bubble rise velocity, $V_B(r)$, is an important parameter to understanding bubble processes, including correctly modeling bubble–sea gas exchange. V_B is the terminal or steady state vertical velocity in a stagnant fluid, and bubbles are considered entrained within the flow, i.e., their mo-

Table 1b

Stream name	V_U (cm s^{-1})	S_F	S_L	Mass flux (mmol s^{-1})	Volume flux (cm^3 s^{-1})	Layer mass (mmol m^{-1})	Layer volume (cm^3 m^{-1})
Pulsing	20	1.2	1.7	53.2	22.0	123.1	51.0
Steady	5	4.1	3.1	7.55	3.55	56.8	26.7
Oily	<2	0.55	1.62	1.64	0.68	9.65	4.00

V_U is upwelling velocity, S_F and S_L are the power law dependencies of the bubble emission and layer distributions, respectively.

tion is a superposition of V_B and bulk fluid motions [29]. Thus a bubble rises with a vertical velocity, $V_Z(r)$, that is a combination of V_B and other vertical velocities, such as the upwelling flows, V_U:

$$V_Z(r) = V_U(r) + V_B(r) \quad (5)$$

The upwelling flow arises due to acceleration of the water by the rising bubbles, and has been observed in seeps in the Santa Barbara Channel [30]. Turbulence generated by both the rising bubbles and the upwelling flow further complicates bubble behavior since a bubble in a turbulence flow is in an accelerated flow (i.e., the bubble is not 'entrained within the flow'). Further complications in $V_Z(r)$ can arise from the accumulation or loss of surfactants as a bubble rises and dissolves or grows. Changes in surface contamination alter V_B because V_B is strongly affected by the presence of surfactants [31] and oil is a powerful surfactant. Thus, $V_Z(r)$ contains considerable information about the bubble's surface state, which in addition to influencing V_B, also strongly affects the bubble gas transfer rate. Furthermore, $V_Z(r)$ is necessary for calculation of $\Psi(r,t)$ from $N(r,t)$. Determination of V_U is complicated in the presence of strong upwelling flows as it varies within the rising stream, decreasing to near zero at the edges [32]. V_U also varied strongly with time in the pulsing plume, whereas the steady plume did not.

Fig. 3 shows $V_Z(r)$ for the three bubble plumes studied. Details of the analysis are shown in Table 2. Of the three, the simplest analysis was for the oily bubble plume because its V_U was the smallest (estimated at <2 cm s^{-1}). Calculated V_Z for the oily plume is shown in Fig. 3c along with the V_B parameterization for clean bubbles [9] and dirty bubbles [10] at 5°C. Also shown is a third-order polynomial fit to $V_Z(r)$. Variability in V_B was probably primarily due to the degree of bubble oiliness, rather than sizing errors since V_Z is only weakly dependent upon r over most of the observed size range. If one assumes that the dirty V_B parameterization is appropriate, then the observation that V_Z values are even lower can only be explained by decreased buoyancy from oil. The increase in the disparity between the dirty V_B parameterization and V_B for 5500-μm bubbles versus 3000-μm bubbles supports the visual observation that larger bubbles were oilier and hence had reduced buoyancy.

The estimates for V_Z for the edge and center of the steady plume are plotted in Fig. 3a. Bubbles in the plume center generally rose faster than equivalently size bubbles at the edge. It was also observed that bubbles in the center were generally larger. For this plume, variability in V_Z probably resulted primarily from turbulence in the upwelling flow. Judging from the regularity of the bubble outlines, it is likely that these bubbles were also significantly contaminated by oil. For 2500-μm bubbles, V_Z at the edge was similar to V_Z in the pulsing plume, discussed below. Thus, based on a comparison between V_Z for 2000–3000-μm bubbles at the plume's edge and center, and assuming bubble oiliness is similar for 2000–3000-μm bubbles in the plume center and edge, V_U was ~ 5 cm s^{-1}. For larger bubbles in the steady plume, oiliness decreased with size. For example, using $V_U = 5$ cm s^{-1}, a 5000-μm bubble rises in the steady plume at about the dirty V_B parameterization, significantly greater than V_B for similar bubbles in the oily bubble plume. Determination of V_U by comparison with the dirty bubble V_B parameterization is not feasible without knowing the amount and effect of oil on bubble buoyancy and hydrodynamics. A least-squares, linear re-

Table 2
Coefficients of vertical velocity, V_Z, and upwelling velocity, V_U, as a function of bubble radius, r, in μm

Stream name	Bubbles analyzed	V_U (cm s^{-1})	V_Z (cm s^{-1})
Pulsing	all	20	$11.9+9.3\times10^{-3}r-5.3\times10^{-7}r^2$
Steady	center	5	$6.51+3.0\times10^{-3}r$
Oily	all	<2	$-0.091+0.0090r-1.22\times10^{-6}r^2$

Not valid for $r > 5000$ μm.

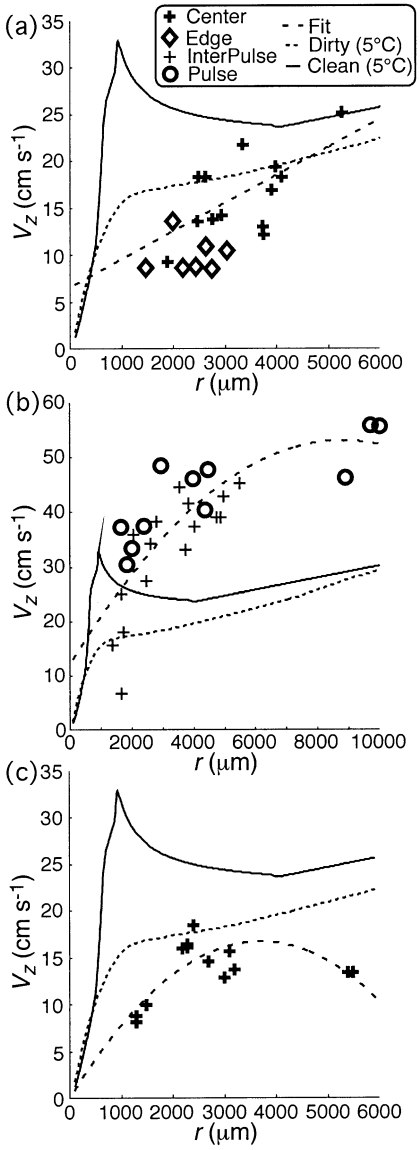

Fig. 3. Bubble vertical velocities, V_Z, observed in the (a) steady stream for the center and edge, (b) pulsing stream during and between pulses, and (c) for the oily stream. Also shown are polynomial fits, and parameterization of rise velocity for clean and dirty bubbles. Data key on figure.

gression fit to V_Z for bubbles in the plume center (which comprised the vast majority of bubbles) is shown in Fig. 3a.

Much higher values for V_Z were observed for the pulsing plume and are shown in Fig. 3b. Bubbles in between pulses generally rose slower. The 1700-μm 'bubble' with $V_Z = 8$ cm s^{-1} probably was an entrained oil droplet. Values of V_Z were generally significantly higher than in the other two plumes. For $r > 3000$ μm, bubbles rose ~ 20 cm s^{-1} faster than the clean V_B parameterization. Both the greater buoyancy of this plume and the presence of many very large bubbles probably caused the greater V_Z and hence stronger V_U. The decrease in V_Z for some of the smallest bubbles may have partly resulted from turbulence eddy trapping; highly erratic motions were observed for these bubbles. It is also interesting to note that the fast moving bubble pulses, which were led by the largest (i.e., fastest) bubbles, were preceded by several centimeters fast moving water as evidenced by sudden acceleration of smaller bubbles. Presumably, the bubble pulse created a bow-wave type flow. A third-order polynomial fit to V_Z for all bubbles (because the pulse/inter-pulse partitioning of bubbles was roughly even) is shown in Fig. 3b.

3.3. Stream distributions

Video sequences of the bubble plumes were digitized, analyzed, and the layer and flux distributions calculated. Fig. 4a shows Φ and Ψ for the pulsing plume, time averaged over several pulses. Bubbles were observed over a size range of $10^3 < r < 10^4$ μm, with a gentle roll-off for $r < 1500$ μm. The absence of a sharp roll-off below the lower r limit suggests bubbles smaller than 1000 μm were present as well. The small r roll-off most likely resulted from bubble streaking, which is worst near the resolution limit. Many very large bubbles were also observed, the largest was $r \sim 1$ cm; however, these very large bubbles were observed to break apart into a few bubbles within a few tenths of a second, sometimes after having just coalesced from several smaller bubbles. Values for Φ decreased gradually, $\Phi \sim r^{-1.69}$ for $r < 5400$ μm, while for larger bubbles, Φ decreased quite steeply, with $S_L = 4.7$. In fact, Φ for the pulsing plume was similar to Φ commonly observed for breaking surface wave bubble plumes [33], which resulted from the break-up of very large bubbles. Thus a similar

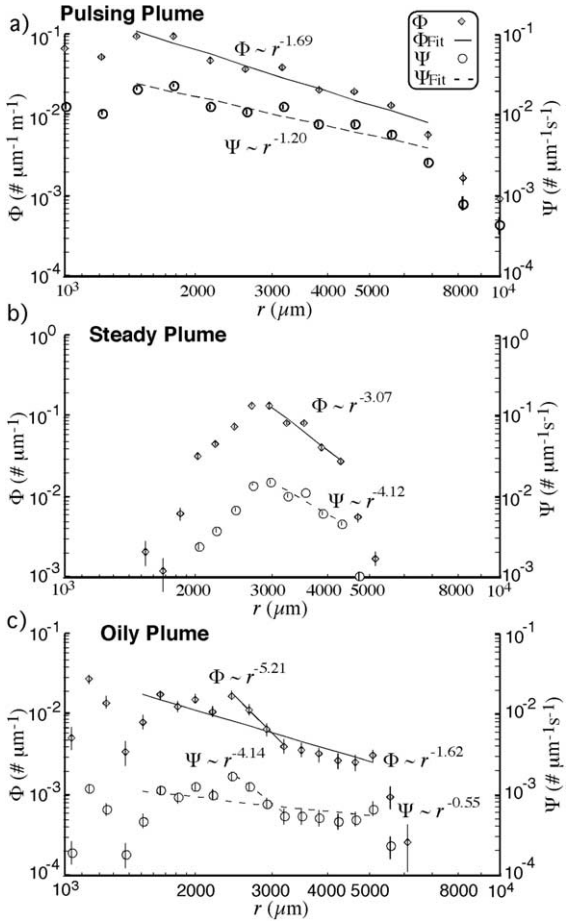

Fig. 4. Bubble layer size distribution, Φ, and bubble flux emission distribution, Ψ, versus radius, r, several meters above the sea bed for the three bubble plumes described in Table 1a and b. Error bars indicated by vertical line lengths, shown for $N > 2$ where N is the number of bubbles in each bin, see text. Data key on (a).

mechanism may be responsible for these bubbles. Integrating Φ over r yields a total of 50 cm^3 of gas per each meter of depth, or 0.123 mol m^{-1} (see Table 1a and b). The flux decreased more gradually from the same peak at $r \sim 1500$ μm with $S_F = 1.2$, as a consequence of the fact that larger bubbles rise faster.

Calculated Φ and Ψ for the steady plume are shown in Fig. 4b, and are very different from those for the pulsing plume (Fig. 4a). The distribution is quite narrow, with a peak at ~ 2700 μm. Bubbles larger than this peak decreased steeply with $S_L = 3.1$. Ψ was steeper, with $S_F = 4.1$. For $r > 4500$, Φ and Ψ decreased significantly more steeply.

A significantly oilier bubble plume was also observed at the Bush Hill site. This bubble plume was created by drilling small holes into exposed deposits of gas hydrate (Plate 1f). During the drilling operation, bubbles, fluid, and oil drops ~ 1 cm in diameter were observed flowing out of the bore hole. The high V_Z of these droplets indicates a buoyancy greater than that of oil, i.e., there probably were internal gas bubbles (discussed below). Images of the oily bubble plume, side illuminated by the collimated light source, are shown in Plate 1g. The degree of oiliness is indicated by the regular, ellipsoid outlines of these bubbles. Due to the side illumination, bubbles appeared as half moons and the error in estimating r was greater because the precise location of the far edge was uncertain. This uncertainty was greatest for smaller bubbles. A reasonable size measurement error is about 25% for small bubbles. For comparison, the size variability of the larger bubbles is ca. 10%, i.e., ± 500 μm for a 5000-μm bubble [34].

The calculated Φ and Ψ for the oily plume are shown in Fig. 4c. This plume consisted of three or four bubble lines, each of which comprised a distinct mode in the bubble size distribution. N was significantly less than for the other plumes, causing greater error. The overall Φ decreased in a manner similar to the pulsing plume, with $S_L = 1.62$, but this is coincidental as Φ resulted from the superposition of Φ from multiple vents. For example, one vent produced a peak at $r \sim 2500$ μm, and decreased very steeply, with $S_L = -5.21$. the overall Ψ is almost flat, with $S_F = 0.55$.

These bubble plumes were observed just a few meters above the sea bed. It is likely that after rising an additional few dozens of meters, the largest bubbles will grow due to the decreasing hydrostatic pressure and consequently break-up, while the smallest bubbles will dissolve [9], narrowing the range of the bubble size distribution.

The bubble distributions can be used to calculate mass and volume distributions to understand which bubble size ranges are most important in

terms of vertical mass transport, or void fraction. Naturally which size ranges are important depends upon the question being asked. If one is looking at bubble dissolution, a different answer may result. The layer volume distribution, Φ_V, for the three plumes are shown in Fig. 5a, the emission mass flux, Ψ_M, is shown in Fig. 5b. One effect of the shallowness of Φ for the oily and pulsing plumes is that due to the cubic dependency of bubble mass on r, most of the mass and volume is contained in the largest bubbles, with Φ_V increasing as $r^{+1.3}$ and $r^{+1.4}$ respectively. Also interesting is that in the range $2500 < r < 3700$ μm, the Φ_V for the steady plume is greater than the pulsing plume, although thanks to the presence of larger bubbles, total Φ_V for the pulsing plume is twice that of the steady plume (Table 1a and b). Similar trends are seen in flux, with most of the mass contained in the larger bubbles, and Ψ_M increasing with r. The increase is steeper than

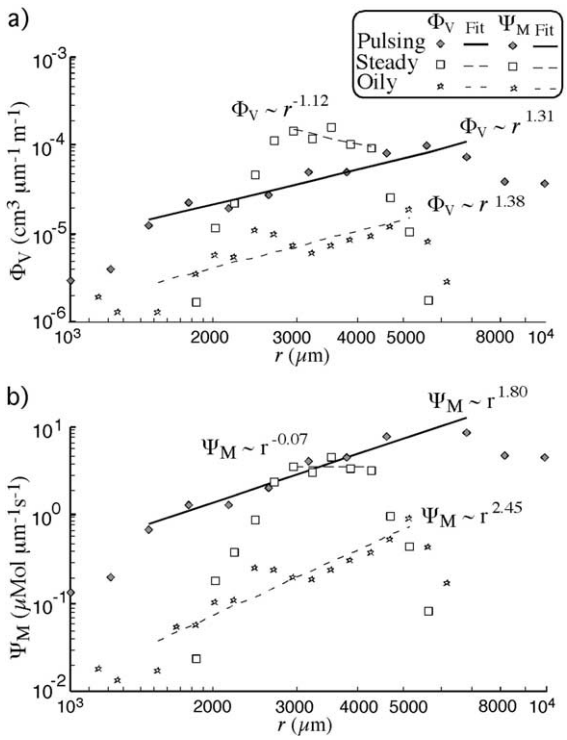

Fig. 5. (a) Bubble layer size volume distribution, Φ_V, and (b) bubble mass emission size distribution, Ψ_M, versus radius, r, for Φ and Ψ shown in Fig. 4. Also shown are fits to the data over the range of the fit. Data key on (a).

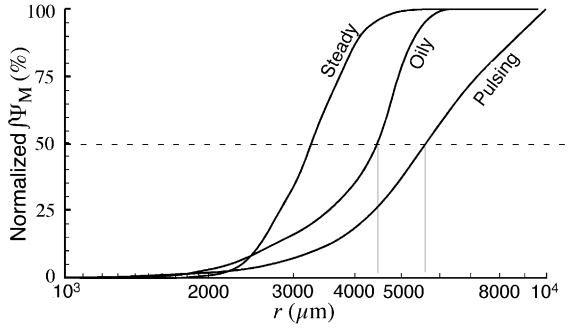

Fig. 6. Normalized, cumulative emission mass flux, $\int\Psi_M$, for the three bubble streams. Streams labeled on figure.

for Φ_V because of the increase of $V_Z(r)$ with r. Also, thanks to $V_Z(r)$ and the different size distributions, the difference in Ψ_M between plumes is greater. For example, total Ψ_M for the pulsing plume is seven times that of the steady plume.

Assuming the bubbles were pure methane and neglecting compressibility, total integrated mass fluxes were 53.2, 7.55, and 1.64 mmol s^{-1} for the pulsing, steady, and oily plumes, respectively (Table 1a and b). Thus the pulsing plume emitted seven times more gas flux than the steady plume and 32 times more than the oily plume. The normalized, cumulative sum of Ψ_M for each plume is shown in Fig. 6. For the pulsing plume, bubbles larger than 5500 μm contain 50% of Ψ_M. Even for the steady plume, with its peak at 2700 μm, 50% of Ψ_M is due to bubbles larger than 3200 μm. In contrast, bubbles smaller than 2000 μm provided only a few percent of Ψ_M. Thus although the resolution limitations of the optical set-up prevented effective measurement of bubbles smaller than 1500 μm, it is improbable that these bubbles provided a significant fraction of Ψ_M.

4. Discussion

These observations provide several new results. The bubble size distributions for several different bubble plumes were analyzed for one seepage site. Back-lit illumination by use of a simple back plane was adequate to provide useful bubble visualization. Two different seep types were observed. In one, the distribution was wide and bub-

ble break-up was observed (pulsing). The other seep type was steady and produced a narrow bubble size distribution. This is most easily explained by the distribution of pore openings. The size of bubble produced has been related to the mouth size of a capillary tube [35], although it is unlikely that the same relationship exists for a generally irregularly shaped seep mouth. Thus if only a narrow range of pore sizes are active, a narrow distribution would be produced.

Theories invoking rapid dissociation of gas hydrate deposits propose bubbly flows from the deposit through the water column and eventually into the atmosphere, e.g., Kennet et al. [7]. One argument that these authors make is that sudden spikes in atmospheric methane and carbon dioxide must be due to gas hydrate dissociation because terrestrial methane sources, e.g., wetland soils, are formed over time scales much longer than the events. Whether the methane released from gas hydrate is partially sequestered in the water column before reaching the atmosphere will strongly influence the time scales of climate change induced by alteration of atmospheric composition. Most marine gas hydrate deposits are located in water depths exceeding 500 m. At the upper end of this depth range, our results show that the fate of bubbles released from gas hydrate can depend on factors such as bubble size, surfactant contamination, and release rate. In water depths of 1000–2000 m, the likelihood that methane would reach the surface directly depends on the production of very large bubbles and very vigorous flow. Otherwise, most of the methane in the bubbles will dissolve in the water column. However, the depths at which dissolution occurred would similarly affect the residence time in the water column. Over long timescales, bacterial oxidation would remove the methane before it reached the atmosphere. Therefore bubble processes need to be considered when modeling the possible contribution of gas hydrate methane to climate change.

Bubble vertical velocities for several bubble streams at the seepage site were presented. Two of the streams (steady and oily) showed velocities below the dirty V_B parameterization, strongly suggesting that buoyancy was decreased due to oil. While the clean V_B parameterization has been well verified in the laboratory and in natural waters, the dirty V_B parameterization has not (except for small, $r < 300$ μm, bubbles [9]). Rather, it is based on numerical simulations from the early 1960s [36].

Bubbles in the oily stream were observed to have the smoothest outlines, and also the least oscillations. Bubbles in the steady stream were also observed to rise as oily, although less so than the oily stream. Due to bubble streaking, the oscillations for bubbles in the pulsing stream were unclear.

Thus there is corroborating evidence that bubbles in the newly created (by drilling) oily stream were oilier than those in the pre-existing steady stream. Thus when gas hydrate containing oil is disturbed, it is likely to be significantly oilier than ongoing seepage. Oil affects bubbles in several ways. Firstly, the decreased buoyancy due to oil causes the bubbles to rise more slowly. In general, contaminants decrease bubble gas transfer efficiency (i.e., the dissolution rate) [10] thereby enhancing the likelihood of bubble survival to the surface and the release of methane to the atmosphere. The surfactant effect depends upon decreased bubble interface mobility due to the effect of contaminants on bubble surface tension [10], since the quantity of surfactant on the bubble is too small to affect buoyancy. In contrast, oily bubbles demonstrated decreased buoyancy, implying the bubbles are coated with an oil layer. Thus gas transfer becomes a three-phase process including the additional step of diffusing across the oil layer. As a result, gas exchange efficiency will be reduced, perhaps significantly. Therefore, oily bubbles potentially have a greater likelihood of transporting methane to the surface than non-oily bubbles. Because oily gas hydrates appear to be widely distributed across the Gulf of Mexico continental slope, the affect on gas dissolution following its release from gas hydrates is an important subject for future study.

Upwelling flows were observed for the steady and pulsing bubble plumes, and V_U was faster for the plume with larger Ψ (i.e., pulsing). It is not known if the upwelling flows persisted to the surface. In shallow seeps in the Santa Barbara

Channel (70 m) surface upwelling flows have been observed [30]. By decreasing the time to reach the surface, upwelling flows also have the potential to significantly decrease methane dissolution, and thus increase transport to the atmosphere, and decrease the depth of dissolution. Furthermore, upwelling flows can transport oil and other particles.

5. Conclusion

Bubbly plumes similar to those observed in this study are a vector that transports hydrocarbons through the water column to the sea surface and to the atmosphere. The dynamics of this process determine the fate of these hydrocarbons. The complex interaction of liquid and gaseous phase hydrocarbons influences the bubbles' rise speed. Varied events can cause shallow deposits of gas hydrate to produce bubbly emissions. The properties of the bubbles and associated fluxes may strongly influence how emitted gases are partitioned between water column and atmosphere. Fundamental understanding of this process can be gained by careful visual measurements of bubble behavior under field conditions. Predicting the fate of hydrate hydrocarbons will require understanding the fate of bubbles in the ocean. To do so requires observations of bubble emission distributions and bubble processes, including the effect of oil. Observations presented show that ignoring oil leads to incorrect characterization of the bubble behavior, and thus predictions. Further observations of bubbles and bubble processes are needed throughout the water column.

Acknowledgements

We are grateful for the facilities and help provided by the crew of the *Johnson Sea Link*. We are thankful for the support of the U.S. Mineral Management Service, U.S. Department of the Interior, under MMS Agreement #1435-01-00-CA-31063 and the National Science Foundation, Ocean Sciences – OCE-0085549 to I.M. The views and conclusions contained in this document are those of the authors and should not be interpreted as necessarily representing the official policies, either expressed or implied, of the U.S. Government.***[BOYLE]***

References

[1] J. Lelieveld, P.J. Crutzen, C. Bruhl, Climate effects of atmospheric methane, Chemosphere 26 (1993) 739–768.
[2] J. Lelieveld, P. Crutzen, F. Dentener, Changing concentration, lifetime and climate forcing of atmospheric methane, Tellus Ser. B-Chem. Phys. Meteor. 50 (1998) 128–150.
[3] K.A. Kvenvolden, Gas hydrates – geological perspective and global change, Rev. Geophys. 31 (1993) 173–187.
[4] W.S. Holbrook, H. Hoskins, W.T. Wood, R.A. Stephen, D. Lizarralde, Leg 164 Science Party, Methane hydrate and free gas on the Blake Ridge from vertical seismic profiling, Science 273 (1996) 1840–1843.
[5] C.K. Paull, W. Ussler III, W.P. Dillion, Is the extent of glaciation limited by marine gas-hydrates?, Geophys. Res. Lett. 18 (1991) 432–434.
[6] M.E. Katz, D.K. Pak, G.R. Dickens, K.G. Miller, The source and fate of massive carbon input during the latest paleocene thermal maximum, Science 286 (1999) 1531–1533.
[7] J.P. Kennett, K.G. Cannariato, I.L. Hendy, R.J. Behl, Carbon isotopic evidence for methane hydrate instability during quaternary interstadials, Science 288 (2000) 128–133.
[8] P.G. Brewer, F.m. Orr, G. Friederich, K.A. Kvenvolden, D.l. Orange, J. McFarlane, W. Kirkwood, Deep-ocean field test of methane hydrate formation from a remotely operated vehicle, Geology 25 (1997) 407–410.
[9] I.S. Leifer, R.K. Patro, The bubble mechanism for transport of methane from the shallow sea bed to the surface: A review and sensitivity study, Cont. Shelf Res. 22 (2002) 2409–2428.
[10] R. Clift, J.R. Grace, M.E. Weber, Bubbles, Drops, and Particles, Academic Press, New York, 1978, 380 pp.
[11] J.M. Brooks, M.C. Kennicutt II, R.R. Fay, T.J. McDonald, R. Sassen, Thermogenic gas hydrates in the Gulf of Mexico, Science 223 (1984) 696–698.
[12] M.C. Kennicutt, J. Sericano, T. Wade, F. Alcazar, J.M. Brooks, High-molecular weight hydrocarbons in the Gulf of Mexico continental slope sediment, Deep-Sea Res. 34 (1987) 403–424.
[13] I.R. MacDonald, N.L. Guinasso Jr., S.G. Ackleson, J.F. Amos, R. Duckworth, R. Sassen, J.M. Brooks, Natural oil slicks in the Gulf of Mexico visible from space, J. Geophys. Res. 98 (1999) 16351–16364.
[14] H. Espedal, T. Wahl, Satellite SAR oil spill detection using wind history information, Int. J. Rem. Sens. 20 (1999) 49–65.
[15] I.R. MacDonald, N.L. Guinasso Jr., J.M. Brooks, R.

Sassen, S. Lee, K.T. Scott, Gas hydrates that breach the sea-floor and interact with the water column on the continental slope of the Gulf of Mexico, Geology 22 (1994) 699–702.

[16] H. Roberts, W. Wiseman Jr., J. Hooper, G. Humphrey, Surficial gas hydrates of the Louisiana continental slope – initial results of direct observations and in situ data collection, in: Offshore Technology Conference 10770, Offshore Technology Conference, Houston, TX, 1999, pp. 259–272.

[17] I.R. MacDonald, D. Buthman, W.W. Sager, M.B. Peccini, N.L. Guinasso Jr., Pulsed oil discharge from a mud volcano, Geology 28 (2000) 907–910.

[18] I.R. MacDonald, G.S. Boland, J.S. Baker, J.M. Brooks, M.C. Kennicutt II, R.R. Bidigare, Gulf of Mexico chemosynthetic communities II: spatial distribution of seep organisms and hydrocarbons at Bush Hill, Mar. Biol. 101 (1989) 235–247.

[19] I.R. MacDonald, J. Guinasso, N.L., J.F. Reilly, J.M. Brooks, W.R. Callender, S.G. Gabrielle, Gulf of Mexico hydrocarbon seep communities VI. Patterns of community structure and habitat, Geol. Mar. Lett. 10 (1990) 244–252.

[20] E.D. Sloan, Clathrate Hydrates of Natural Gases, Marcel Dekker, New York, 1990, 641 pp.

[21] R. Sassen, I.R. MacDonald, N.L. Guinasso Jr., S. Joye, A.G. Requejo, S.T. Sweet, J. Alcala-Herrera, D.A. DeFritas, D.R. Schink, Bacterial methane oxidation in sea-floor gas hydrate: significance to life in extreme environments, Geology 26 (1998) 851–854.

[22] R. Sassen, I. MacDonald, A. Requejo, N. Guinasso, M. Kennicutt II, S. Sweet, J. Brooks, Organic geochemistry of sediments from chemosynthetic communities, Gulf of Mexico slope, Geol. Mar. Lett. 14 (1994) 110–119.

[23] National Institutes of Health, NIH Image ver. 1.62b30 2000, National Institutes of Health, 2000.

[24] J. Russ, The Image Processing Handbook, Boca Raton, FL, 1998, 771 pp.

[25] I. Leifer, G. De Leeuw, L.H. Cohen, Optical measurement of bubbles: system design and application, J. Atmos. Ocean. Tech. (2002) in press.

[26] A. Sam, C.O. Gomez, J.A. Finch, Axial velocity profiles of single bubbles in water/froth, Int. J. Min. Process 47 (1996) 177–196.

[27] B.D. Johnson, R.C. Cooke, Bubble populations and spectra in coastal waters: a photographic approach, J. Geophys. Res. 92 (1979) 3761–3766.

[28] H. Medwin, N.D. Breitz, Ambient and transient bubble spectral densities in quiescent seas and under spilling breakers, J. Geophys. Res. 94C (1989) 12751–12759.

[29] D.K. Woolf, S.A. Thorpe, Bubbles and the air–sea exchange of gases in near saturation conditions, J. Mar. Res. 49 (1991) 435–466.

[30] I. Leifer, J. Clark, R. Chen, Modifications of the local environment by a natural marine hydrocarbon seep, Geophys. Res. Lett. 27 (2000) 3711–3714.

[31] R. Patro, I. Leifer, P. Bowyer, Better bubble process modeling: Improved bubble hydrodynamics parameterisation, in: M. Donelan, W. Drennan, E.S. Salzman, R. Wanninkhof (Eds.), Gas Transfer and Water Surface, AGU Monograph 127 (2001) 315–320.

[32] T.J. McDougal, Bubble plumes in stratified environments, J. Fluid Mech. (1978) 655–672.

[33] I. Leifer, G. De Leeuw, Bubble measurements in breaking-wave generated bubble plumes during the LUMINY wind-wave experiment, in: M. Donelan, W. Drennan, E.S. Salzman, R. Wanninkhof (Eds.), Gas Transfer and Water Surface, AGU Monograph 127 (2001) 303–309.

[34] I. Leifer, R. Patro, P. Bowyer, A study on the temperature variation of rise velocity for large clean bubbles, J. Atmos. Ocean. Tech. 17 (2000) 1392–1402.

[35] D.C. Blanchard, L.D. Syzdek, Production of air bubbles of a specified size, Chem. Eng. Sci. 32 (1977) 1109–1112.

[36] D.W. Moore, The boundary layer on a spherical gas bubble, J. Fluid Mech. 16 (1963) 161–176.